Comparison Between Numerical and Experimental Results on Mechanical Stirrer and Bubbling in a Cylindrical Tank – 13047

M. Lima da Silva*[1], A. Gagnoud**, Y. Fautrelle**, E. Sauvage*, P. Brun* and R. Riva***
* CEA-Marcoule, BP 17171, 30207 Bagnols sur Cèze, France
** SIMaP, Grenoble INP, UJF, CNRS, BP 75, 38402 Saint Martin D'Hères, France
*** CEA-Grenoble, 17 rue des Martyrs, 38054 Grenoble, France

ABSTRACT

The process of vitrification in a cold crucible heated by direct induction is used in the fusion of oxides. Its feature is the production of high-purity materials. The high-level of purity of the molten is achieved because this melting technique excludes the contamination of the charge by the crucible. The aim of the present paper is to analyze the hydrodynamic of the vitrification process by direct induction, with the focus in the effects associated with the interaction between the mechanical stirrer and bubbling. Considering the complexity of the analyzed system and the goal of the present work, we simplified the system by not taking into account the thermal and electromagnetic phenomena. Based in the concept of hydraulic similitude, we performed an experimental study and a numerical modeling of the simplified model. The results of these two studies were compared and showed a good agreement. The results presented in this paper in conjunction with the previous work contribute to a better understanding of the hydrodynamics effects resulting from the interaction between the mechanical stirrer and air bubbling in the cold crucible heated by direct induction. Further works will take into account thermal and electromagnetic phenomena in the presence of mechanical stirrer and air bubbling.

INTRODUCTION

The cold crucible melter vitrification technology heated by direct induction has a water-cooling system. This system is responsible for cooling the melter wall. The cooling of the melter wall produces a solidified glass layer that protects the melter inner wall from corrosion. The cold crucible melter has two mechanisms of forced convection: the mechanical stirrer and air bubbling. These two mechanisms are optimized to ensure thermal and chemical homogeneity.

The aim of the present paper is to analyze the hydrodynamics of the vitrification process by direct induction, and to study the effects associated with the interaction between the mechanical stirrer and bubbling. As we are interested only in the study of the hydrodynamics of the process and due to complexity of the analyzed system, we decided to simplify the problem by not taking into account the thermal and electromagnetic effects. As a consequence, based in the concept of hydrodynamic similitude, we performed an experimental study and a numerical modeling of the simplified model. In this work, we adopted a silicon oil of viscosity equivalent to the molten

[1] corresponding author: marcio.lima-da-silva@simap.grenoble-inp-fr, +(33) 4 76 82 52 61, +(33) 4 76 82 52 49

glass (1~10 Pa.s), because the physical properties of the glass strongly depend on the temperature field. We used the hydrodynamic similitude to ensure the equivalence between the real and the simplified model of the cold crucible melter.

THE EXPERIMENTAL STUDY

The experimental results presented in this work were obtained from a study realized in hydrodynamic similitude. In this experiment, we used a cylindrical tank filled with silicon oil. This tank had a diameter on the order of 0.5 m and it was equipped with a mechanical stirrer and nozzles for the air bubbling. The mechanical stirrer had a 0.390 m of span, 11° of tilt, and a rectangular section of 0.05 x 0.02 m. The nozzles were located in the bottom of the tank. The experiments were performed varying the angular velocity of the mechanical stirrer between 0, 20, 40 and 60 rpm for air injection rates of 0 and 1225 l/h. The details of this tank are presented in Fig. 1.

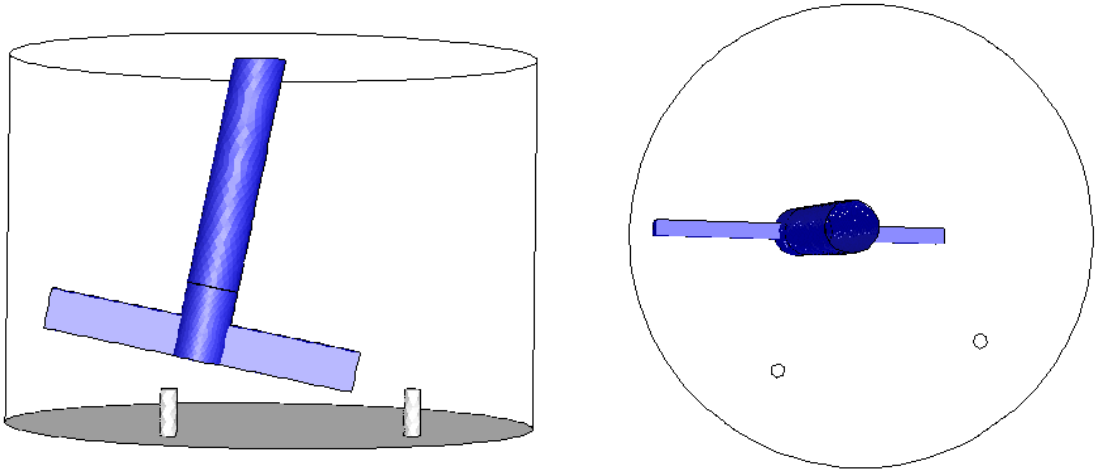

(a) (b)

Fig. 1. Schematic view of the cylindrical tank with the mechanical stirrer and the air bubbling system. Fig. 1(a). Front view of the tank. Fig. 1(b). Upper view of the tank.

THE NUMERICAL STUDY

We conducted a numerical modeling of the experimental study described above. The flow was assumed to be unsteady laminar. The simulations were realized for the four agitation speeds and the two air injection rates. The geometry was created in the commercial code GAMBIT®[2]. The numerical simulations were performed by the means of the finite volume commercial code FLUENT®[3]. We carried out 3D simulations of the simplified model. The Sliding Mesh method was selected for the modeling of the mechanical stirring and we developed an equivalent force

[2] *GAMBIT® is a registered trademark of ANSYS, Inc.*

[3] *FLUENT® is a registered trademark of ANSYS, Inc.*

model for the agitation by gas bubbling [1,2].

Stirring Modeling

The mechanical stirring modeling was performed using the numerical technique called Sliding Mesh, available in FLUENT® [3]. This technique is used to model mobile grids. Using this method we split the computational domain of the tank in two regions, Fig. 2. The first one is static and represents the tank. The second one is mobile and represents the stirrer with a transition zone between the blades and the static zone. The mechanical stirrer axis was modeled inside the stationary region.

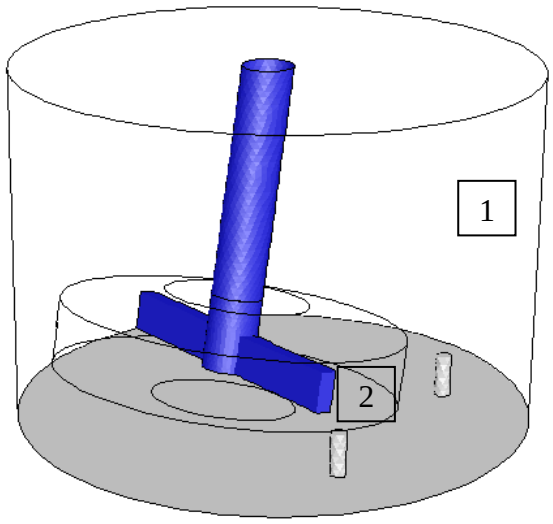

Fig. 2. Visualization of the computational domain of the cylindrical tank with the static (1) and moving (2) regions.

The relation between the absolute velocity ($\vec{u}$), compared to the fixe inertial frame, and the relative velocity ($\vec{u}_r$) related to the rotating frame is showed in (Eq. 1).

$$\vec{u} = \vec{u}_r + \left(\vec{\Omega} \wedge \vec{r}\right) \qquad \text{(Eq. 1)}$$

where $\vec{\Omega}$ is the angular velocity associated with the mechanical stirrer and $\vec{r}$ is the position vector.

The Sliding Mesh technique allows to solve the Navier-Stokes equations considering the inertial frame, (Eq. 2) and (Eq. 3), [4]. This formulation takes in account the effects of the Coriolis acceleration, (Eq. 4), and of the centrifugal acceleration, (Eq. 5). The term $\bar{\bar{\tau}}$, (Eq. 6), represents the stress tensor.

$$\vec{\nabla} \cdot \vec{u}_r = 0 \qquad \text{(Eq. 2)}$$

$$\rho\left(\frac{\partial \vec{u}_r}{\partial t} + (\vec{u}_r \cdot \vec{\nabla})\vec{u}_r\right) + 2\vec{\Omega} \wedge \vec{u}_r + \vec{\Omega} \wedge \vec{\Omega} \wedge \vec{u}_r = -\vec{\nabla}p + \vec{\nabla}\bar{\bar{\tau}} + \rho\vec{g} + \vec{F} \qquad \text{(Eq. 3)}$$

$$\vec{a}_{Coriolis} = 2\vec{\Omega} \wedge \vec{u}_r \qquad \text{(Eq. 4)}$$

$$\vec{a} = \vec{\Omega} \wedge \vec{\Omega} \wedge \vec{u}_r \qquad \text{(Eq. 5)}$$

$$\bar{\bar{\tau}} = \vec{\nabla} \cdot \left(\mu\left(\vec{\nabla} \cdot \vec{u}_r + \vec{\nabla} \cdot \vec{u}_r^T\right)\right) \qquad \text{(Eq. 6)}$$

$\vec{F}$ is the body force exercised in the flow by the bubbling (Eq. 3).

Bubbling Modeling

In this work, the bubble trajectory was modeled by the means of an equivalent force model. This model considers the influence of the mechanical stirring to calculate the deviation of the bubble column. The principle is to assume the bubble column's trajectory as a single particle and to determine the velocity field of the flow considering the mechanical stirrer. To carry out this modeling technique, we used Lagrangian single particle tracking, (Eq. 7).

$$\frac{d\overrightarrow{u_p}}{dt} = F_D\left(\vec{u} - \overrightarrow{u_p}\right) + \frac{\vec{g}\left(\rho_p - \rho\right)}{\rho_p} + \vec{F}_{sup} \qquad \text{(Eq. 7)}$$

Where F_D, (Eq. 8), is the drag force factor calculated with the Reynolds number and with the drag coefficient, C_D,

$$F_D = \frac{18\mu}{\rho_p d_p^2}\frac{C_D Re}{24} \qquad \text{(Eq. 8)}$$

and the $\vec{F}_{sup}$, (Eq. 9), represents the virtual mass force, first right term, and the force due to the pressure gradient, second right term.

$$\vec{F}_{sup} = \frac{1}{2}\frac{\rho}{\rho_p}\frac{d}{dt}\left(\vec{u} - \overrightarrow{u_p}\right) + \frac{\rho}{\rho_p}\overrightarrow{u_p}\frac{du}{dx_i} \qquad \text{(Eq. 9)}$$

The Reynolds number, (Eq. 10), was calculated using the equivalent diameter of the bubbles (D_e) obtained from the correlation presented in (Eq. 11) [5].

$$Re = \frac{\left\|\vec{u} - \overrightarrow{u_p}\right\| D_e}{\nu} \quad \text{(Eq. 10)}$$

$$\boldsymbol{D_e = d_0\left(\frac{5}{Bd_0^{1.08}} + \frac{9.261Fr}{Ga^{0.39}} + 2.147Fr^{0.31}\right)^{1/3}} \quad \text{(Eq. 11)}$$

Where d_0 is the diameter of the nozzle and it's equal to 0.004 m. Eq. 11 takes into account the Galilée number, the Bond number and the Froude number to calculate the equivalent diameter of the bubbles.

The body force imposed in the central region of the bubbling column, $\vec{F}$, is given by

$$\vec{F} = \rho_L \vec{g} \varepsilon_G \quad \text{(Eq.12)}$$

and it corresponds to the buoyancy force of the average volume of bubble in the column. This force is calculated using the equivalent diameter of the bubbles (Eq. 11), the gas fraction in the column (Eq. 13), the bubbles velocity (Eq. 14) and the drag coefficient (Eq15) [6,7].

$$\varepsilon_G = \frac{2}{3}\frac{QD_e}{V_B V_{ol}} \quad \text{(Eq.13)}$$

$$C_d = 1 + \frac{16\nu}{V_B D_e} \quad \text{(Eq.14)}$$

$$V_B^2 = \frac{4}{3}\frac{D_e g(1+\varepsilon_G)}{C_d} \quad \text{(Eq.15)}$$

We were motivated to adopt this method instead of a numerical model available in FLUENT®, because it presented a gain in simulation time compared with other models and hence it is more efficient numerically.

Geometry and Mesh

The computational domain was created according to the dimensions of the cylindrical tank used in the experiments. As our goal is to model the flow in the tank without taking in account the free surface between the oil and the air, we simplified the geometry by adopting the experimental free surface level at the initial height of the tank at rest. All others dimensions of the experimental tank were respected in the numerical model. The two subdomains represent the static and the moving zones were created, Fig. 2. Considering the level of complexity of the geometry, we decided to adopt a mesh composed of tetrahedral elements. The element size was chosen in order to provide a good discretization of the geometry. As a result, we obtained a computational domain from the order of 510000 tetrahedral cells, Fig. 3.

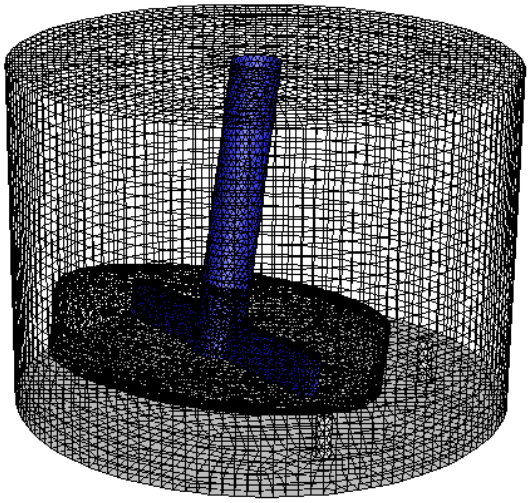

Fig. 3. Mesh grid of the computation domain.

Boundary Conditions

The definition of the boundary conditions was realized considering the hypothesis defined to solve the flow. In general, we adopted at the walls of the domain the no-slip boundary condition. At the walls between the static and the moving volume, we adopted the interface boundary condition. This kind of boundary condition allows the transfer of information between the two subdomains during the simulations.

Convergence Criteria and Simulation Time

The time step was defined taking in account the element size from the interface between the stationary and the moving volume (0.015 m), the moving volume radius (0.215 m) and the mechanical stirrer angular velocity. The condition respected for the time step definition was to allow the maximal displacement of one element per time step. As an example, for an angular velocity equal to 40 rpm, we obtained a time step of 0.015 s. This time step definition allied to the discretization of the computational domain provided to us a cell Reynolds number close to 1.

The calculations were realized in two stages. At the first one, we did not take into account the air bubbling. We carried out the simulations for 10 periods, what was enough to achieve a periodical flow regime. After the periodical regime established, the average flow measurements were collected during 1 period. At the second stage, we added to the system the bubbling deviation. The methodologies used to stabilize the flow and collected the results were the same adopted at the first phase. In the end of each stage, the velocity field was exported to be utilized in the comparison with the experimental results.

As numerical schemes, we adopted the scheme COUPLED for the pressure-velocity coupling,

the scheme PRESTO! for the pressure, the Third Order MUSCL for the momentum and a first order implicit scheme for the transient formulation. The convergence criterion for the equations residual was defined as 10^{-4} for all the equations and it was respected in all cases. The simulations presented in this work took one week to achieve the residual convergence level established using four 3.07 GHz x86 processors.

COMPARISON BETWEEN NUMERICAL AND EXPERIMENTAL RESULTS

We compared the experimental and numerical results for the four angular velocities of the mechanical stirrer and the air injection rates of 0 and 1225 l/h. The experimental results were obtained using the Particle Image Velocimetry technique (PIV) [8]. The flow measurements with the PIV were realized on the plane x = -0.180 m, Fig. 4.

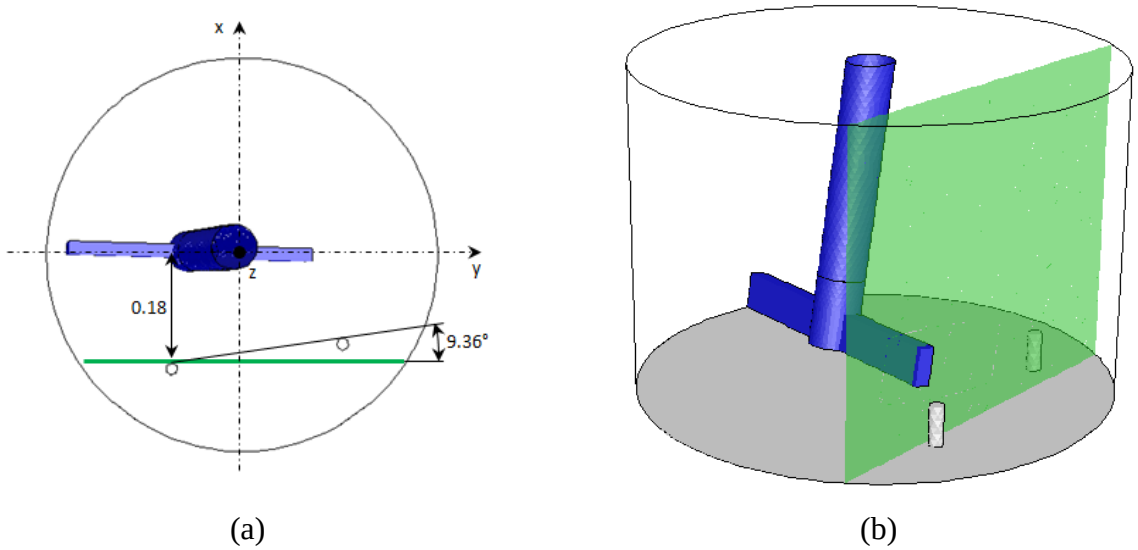

(a) (b)

Fig. 4. Visualization of the plane x = -0.180 m used in the PIV measures. Fig. 4(a). Upper view of the tank. Fig. 4(b). “Shadow area” created by the interference between the plane x = -0.180 m and the mechanical stirrer.

Using this technique, we obtained the average velocity field, the y and z-components velocity on the plane x = -0.180 m in all experimental configurations. The intersection between this plane and the mechanical stirrer influences the PIV measurements creating what we called by “shadow area”. The effect of the “shadow area” in the flow measures was visualized as under speed zones over the velocity field. The same flow measurements were realized at the numerical study.

We carried out two types of comparison between the experimental and numerical results: a qualitative comparison between the average velocity fields and a quantitative comparison between the profiles of the y and z-components of velocity. The two nozzles were represented in the results, but only the one on the left side was used during the experimental and numerical study.

The average velocity field was evaluated for two configurations of air bubbling, the first one was without air injection and the second one was with an air injection rate equal to 1225 l/h. In the first situation, we compared the experimental and numerical results of the averaged velocity field and the profiles for 20, 40 and 60 rpm, Fig. 5. For the air injection of 1225 l/h, we conducted the same kind of comparison for the 0, 20, 40 and 60 rpm, Fig. 6.

These evaluations showed a good agreement between the experimental and numerical results. The effect of the "shadow area" in the experimental results was clearly visualized as an under velocity area in the velocity field.

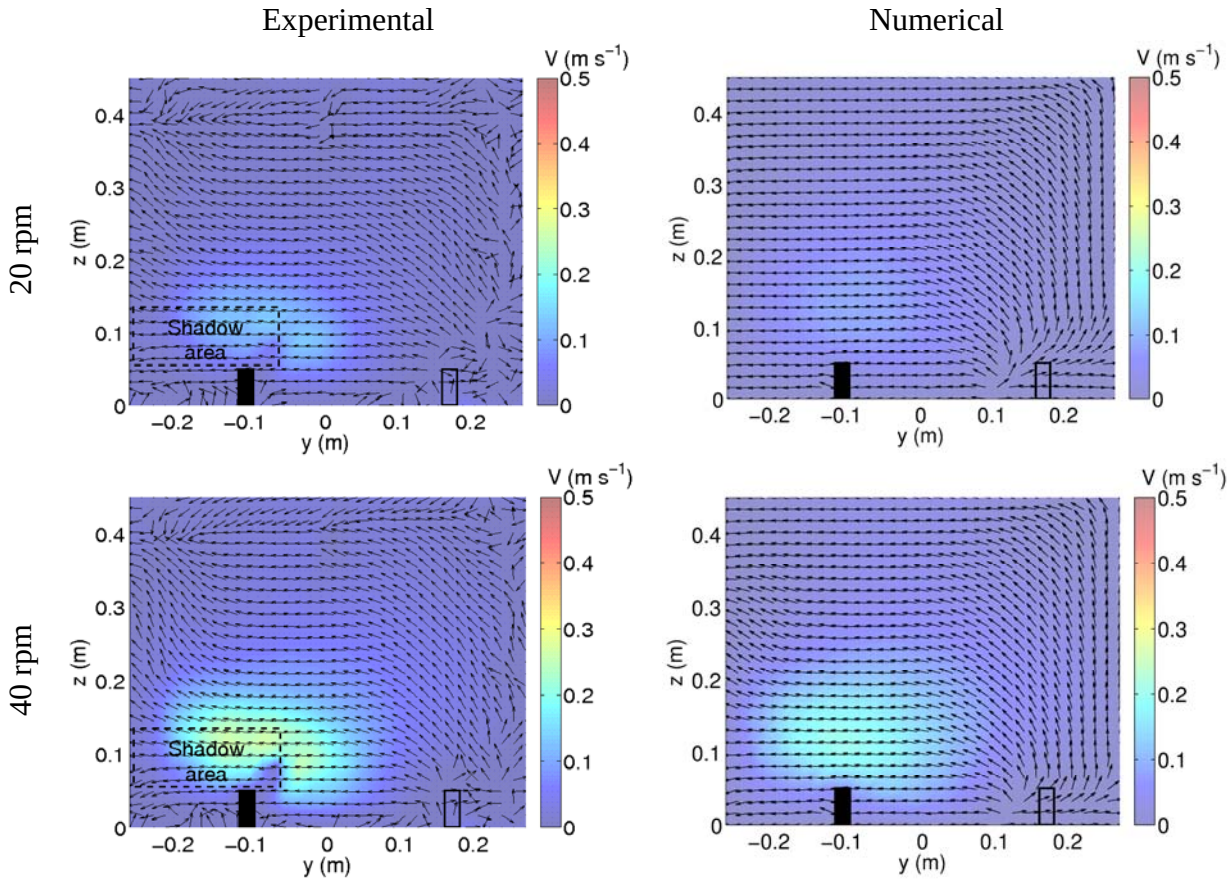

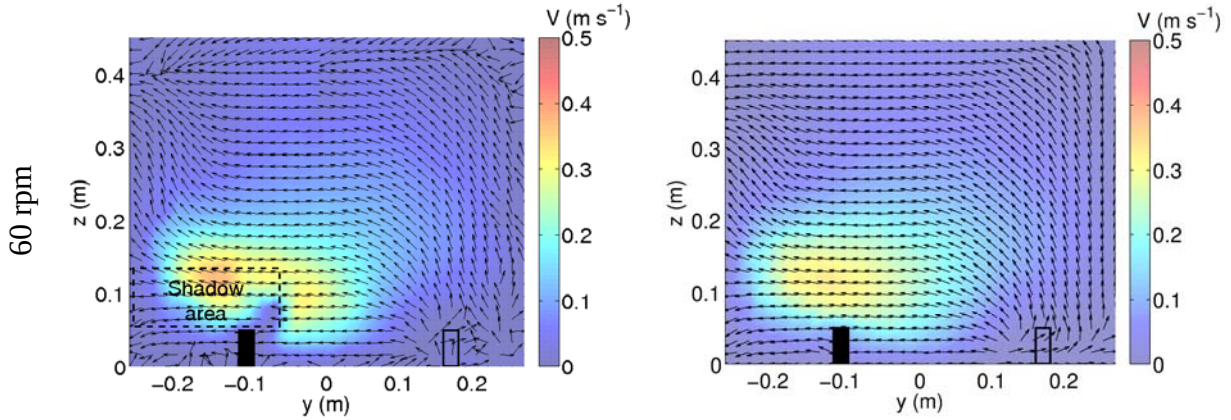

Fig. 5. Comparison between the experimental (left column) and numerical (right column) average velocity field over the plane x = -0.180 m for 20, 40 and 60 rpm without air injection. The nozzles are represented in the bottom of the figures.

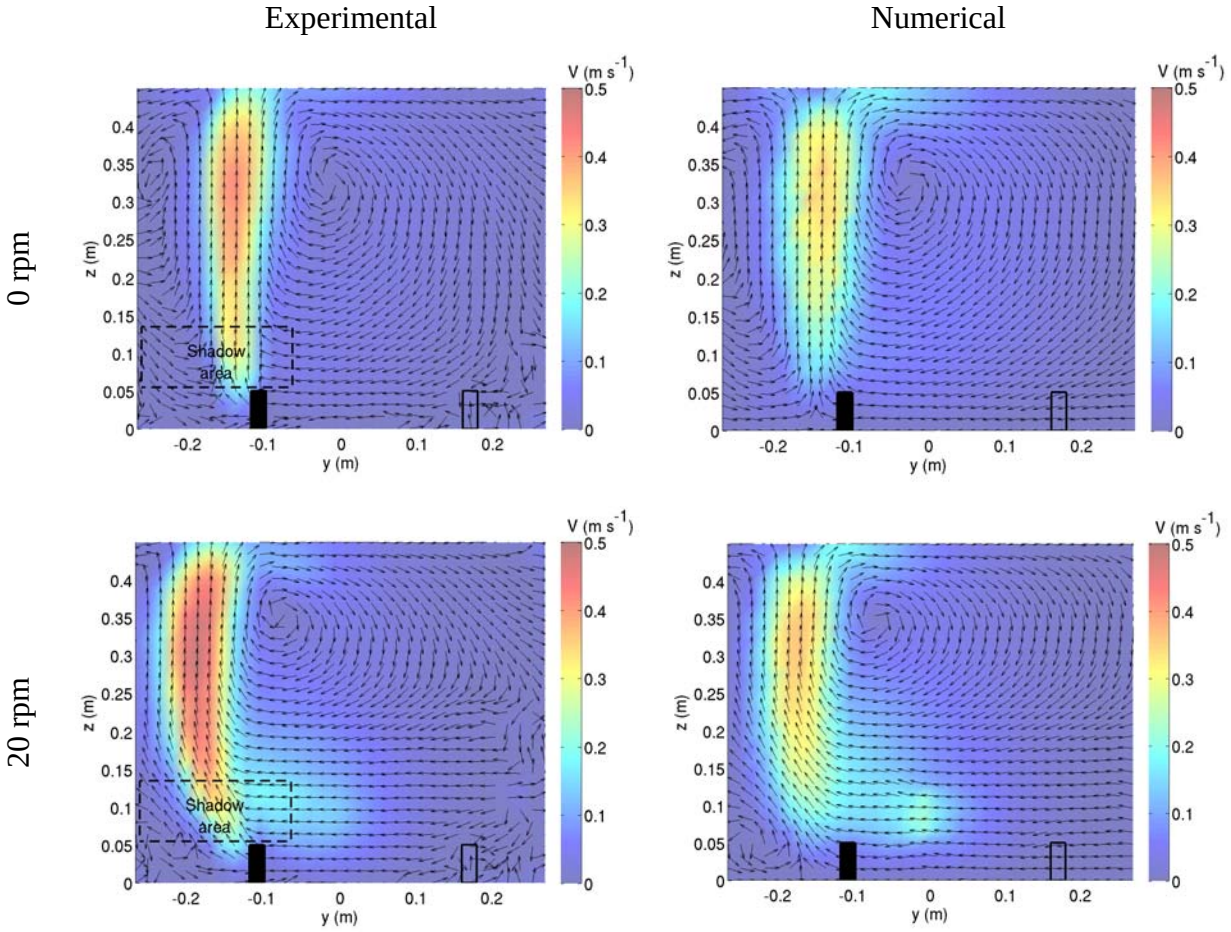

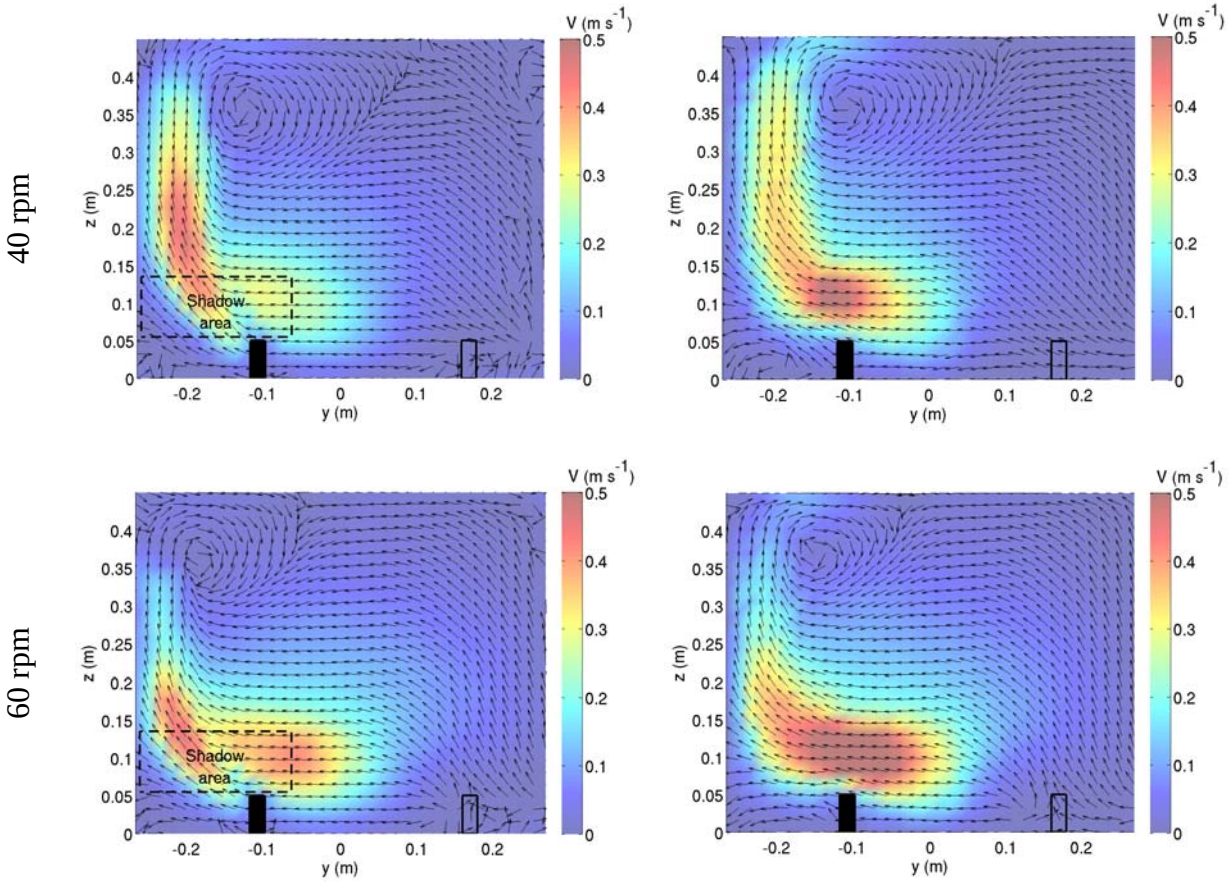

Fig. 6. Comparison between the experimental (left column) and numerical (right column) average velocity field at x = -0.180 m for 0, 20, 40 and 60 rpm for an air injection rate of 1225 l/h. The nozzles are represented in the bottom of the figures and only the left one was used in this work.

The quantitative comparisons between the y and z-components of the average velocity field were performed at the level z = 0.252 m. This level was selected considering a reduction of the effects created by the "shadow area" in the PIV measurements of the average velocity field.

We carried out these evaluations for the two configurations of air bubbling. In the case without air injection, Fig. 7, we noticed a good agreement between the experimental and the numerical profiles of the y and z-components at all the range of angular velocities. In the case with an air injection rate of 1225 l/h, Fig. 8, we observed at the y and z-components a difference between the experimental and numerical results in the region affected by the air bubbling, Fig. 8(a) and Fig. 8(b). This discrepancy is possibly due to that the mesh was not fine enough in that region.

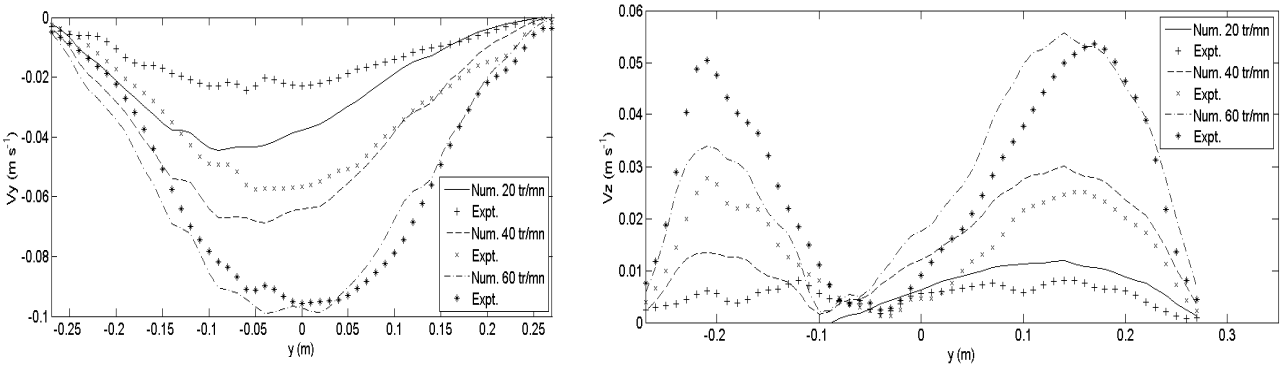

(a) (b)

Fig. 7. Comparison between the experimental and numerical profiles of the y-component, Fig. 7(a), and the z-component, Fig. 7(b), at z = 0.252 m over the plane x = -0.180 m for 20, 40 and 60 rpm and without air injection.

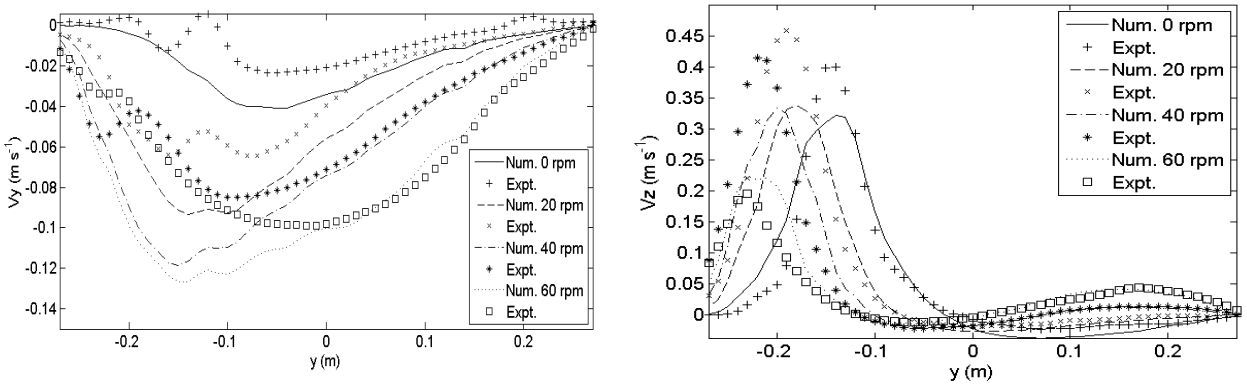

(a) (b)

Fig. 8. Comparison between the experimental and numerical profiles of the y-component, Fig. 8(a), and the z-component, Fig. 8(b), at z = 0.252 m over the plane x = -0.180 m for 0, 20, 40 and 60 rpm and an air injection rate of 1225 l/h.

CONCLUSIONS

The comparison between the numerical and experimental results showed a good agreement. The effect of deviation of bubbles by action of the mechanical stirrer was verified in both results. This paper complements the study about the thermal convection in the cold crucible [9]. The results obtained in this paper in conjunction with the previous work contribute to a better understanding of the hydrodynamics effects resulting from the interaction between the mechanical stirrer and air bubbling in the cold crucible heated by direct induction. The conclusions of the present paper will be used as support in further modeling of the cold crucible melter. These future simulations will take into account thermal and electromagnetic effects in the presence of mechanical stirrer and air bubbling.

APPENDIX A

Nomenclature

$\vec{a}$ = centrifugal acceleration

$\vec{a}_{Coriolis}$ = Coriolis acceleration

d_p= particle diameter

d_0 = diameter of the nozzle

$\vec{f}$ = body force of the bubbling

$\vec{g}$ = acceleration of gravity

p = pressure

$\vec{r}$ = position vector

$\vec{u}$ = absolute velocity vector

$\overrightarrow{u_p}$ = particle velocity vector

$\vec{u}_r$ = relative velocity vector

C_D = drag coefficient

D_e = equivalent bubble diameter

F_D = drag force

B = Bond number

Fr = Froude number

Ga = Galilée number

Q = gas injection rate

Re = Reynolds number

V_B = bubble velocity

V_{ol} = volume of a bubble

Greek letters

$\vec{\Omega}$ = vector angular velocity

$\bar{\bar{\tau}}$ = tensor stress

μ = dynamic viscosity

ε_G = gas fraction

ν = cinematic viscosity

ρ = density

ρ_p = particle density

ρ_L = liquid density

REFERENCES

1. E. SAUVAGE, "Modélisation numérique thermo-hydrodynamique et inductive d'une fonte verrière élaborée en creuset froid inductif", PhD Thesis, 2009.

2. E. SAUVAGE, A. BONNETIER, D. GAUTHERON, P. BRUN, J. LACOMBE. "*Numerical simulation of vitrification processes: glass homogeneity by gas bubbling study*". Procedia Chemistry, 7, 593-598, 2012.

3. FLUENT®, User's Guide, 2006.

4. G. K. BATCHELOR, "*An Introduction to Fluid Dynamics*", Cambridge University Press, 2000.

5. M. JAMIALAHMADI, M. ZEHTABAN, H. MÜLLER-STEINHAGEN, A. SARRAFI and J. SMITH, "Study of bubble formation under constant flow conditions", Chemical Engineering Research and Design, 75(5):532, 2001.

6. P. SNABRE and F. MAGNIFOTCHAM: I. "*Formation and rise of a bubble stream in a viscous liquid*". The European Physical Journal B, 4:369–377, 1998.

7. P. SNABRE and F. MAGNIFOTCHAM : II. "*Recirculation flow induced by a bubble stream rising in a viscous liquid*". The European Physical Journal B, 4:379–386, 1998.

8. K. D. JENSEN, "Flow Measurements", *Journal of the Brazilian Society of Mechanical Sciences and Engineering*, **XXVI**(4), 2004.

9. P. BRUN, E. SAUVAGE, E. CHAUVIN. "*3-D Thermal, hydrodynamic and magnetic modelling of elaboration of glass by induction in cold crucible*". Waste Management, WM 2009 Conference, March 1-5, 2009, Phoenix, Arizona.